nature physics

LETTERS

https://doi.org/10.1038/s41567-018-0058-3

Alfvén wave dissipation in the solar chromosphere

Samuel D. T. Grant[1*], David B. Jess[1,2], Teimuraz V. Zaqarashvili[3,4,5], Christian Beck[6], Hector Socas-Navarro[7,8], Markus J. Aschwanden[9], Peter H. Keys[1], Damian J. Christian[2], Scott J. Houston[1] and Rebecca L. Hewitt[1]

Magnetohydrodynamic Alfvén waves[1] have been a focus of laboratory plasma physics[2] and astrophysics[3] for over half a century. Their unique nature makes them ideal energy transporters, and while the solar atmosphere provides preferential conditions for their existence[4], direct detection has proved difficult as a result of their evolving and dynamic observational signatures. The viability of Alfvén waves as a heating mechanism relies upon the efficient dissipation and thermalization of the wave energy, with direct evidence remaining elusive until now. Here we provide the first observational evidence of Alfvén waves heating chromospheric plasma in a sunspot umbra through the formation of shock fronts. The magnetic field configuration of the shock environment, alongside the tangential velocity signatures, distinguish them from conventional umbral flashes[5]. Observed local temperature enhancements of 5% are consistent with the dissipation of mode-converted Alfvén waves driven by upwardly propagating magneto-acoustic oscillations, providing an unprecedented insight into the behaviour of Alfvén waves in the solar atmosphere and beyond.

The solar surface hosts a web of diverse magnetic fields, from sunspots exhibiting sizes that dwarf the Earth, to dynamic bright grains only a few hundred kilometres across. The magnetic nature of the Sun's atmosphere supports the plethora of magnetohydrodynamic (MHD) wave activity observed in recent years[6]. Such wave motion is predominantly generated near the surface of the Sun, with the creation of upwardly propagating MHD waves providing a conduit for the transportation of heat, from the vast energy reservoir of the solar photosphere, to the outermost extremities of the multi-million-degree corona.

In comparison to other MHD modes, Alfvén waves are the preferred candidates for energy transport since they do not reflect or dissipate energy freely[3]. Observational studies have been limited by the challenging requirements on instrumentation needed to identify the Doppler line-of-sight (LOS) velocity perturbations and non-thermal broadening associated with Alfvén waves, thus there is only tentative evidence of their existence within the Sun's magnetized plasma[7–9]. Given the difficulties associated with resolving the intrinsic wave signatures, to date there has been no observational evidence brought forward to verify the dissipative processes associated with Alfvén waves.

Theoretical studies have proposed multiple dissipation methods that would allow the embedded mechanical energy of Alfvén waves to be converted into localized heat[10,11]. Unfortunately, most act on unobservable scales, providing no clear signatures that can be identified with even the largest current solar telescopes. However, one distinct mechanism revolves around the formation of macroscopic shock fronts, which naturally manifest as a result of the propagation of waves through the solar atmosphere[12]. Shock behaviour induced by slow magneto-acoustic waves is ubiquitously observed in sunspots, manifesting as umbral flashes[5] (UFs), giving rise to notable periodic intensity and temperature excursions[13]. Importantly, from a theoretical viewpoint, the shock dissipation of propagating wave energy also applies to Alfvén waves[14]. Here, large-amplitude linearly polarized Alfvén waves induce their own shock fronts[15], or the associated ponderomotive force of propagating Alfvén waves leads to the excitation of resonantly shocked acoustic perturbations[16]. In this Letter, we present unique high-resolution observations and magnetic field extrapolations, combined with thermal inversions and MHD wave theory, to provide first-time evidence of Alfvén wave dissipation in the form of shock fronts manifesting close to the umbral boundary of a sunspot.

Intensity scans of the chromospheric Ca II 8,542 Å spectral line at high spatial (71 km per pixel) and temporal (5.8 s) resolution were conducted for a $70\times70\,\mathrm{Mm}^2$ region centred around a large sunspot on 24 August 2014 using the Interferometric BIdimensional Spectrometer[17] (IBIS) at the Dunn Solar Telescope. Three-dimensional values for the vector magnetic field are derived through nonlinear force-free extrapolations[18] applied to simultaneous magnetograms obtained by the Helioseismic and Magnetic Imager[19] (HMI) aboard the Solar Dynamics Observatory (SDO) spacecraft. The resulting images (Fig. 1) highlight the connectivity between the magnetic fields and the structuring of the sunspot atmosphere. Intensity thresholding of running-mean-subtracted images of the chromospheric umbra allowed for the identification of 554,792 individual shock signals across the 135 minute duration of the dataset.

The sunspot displays a classical structure, providing two preferential locations for plasma shock formation in the umbra: first, in the vicinity of strong, vertical magnetic fields near the umbral centre of mass, and second, in the presence of weaker, inclined fields towards the outer boundary of the umbra (Fig. 2). The first population is attributed to UFs, whereby the near-vertical propagation of magneto-acoustic waves across multiple density scale heights promotes their efficient steepening into shocks[20]. The second population, whose intensity excursions are formed along inclined magnetic fields that channel waves almost horizontally (inclinations of approximately 70–80 degrees), provides the first indication of

[1]Astrophysics Research Centre, School of Mathematics and Physics, Queen's University Belfast, Belfast, UK. [2]Department of Physics and Astronomy, California State University Northridge, Northridge, CA, USA. [3]Space Research Institute, Austrian Academy of Sciences, Graz, Austria. [4]Abastumani Astrophysical Observatory at Ilia State University, Tbilisi, Georgia. [5]Institute of Physics, IGAM, University of Graz, Graz, Austria. [6]National Solar Observatory (NSO), Boulder, CO, USA. [7]Instituto de Astrofísica de Canarias, La Laguna, Spain. [8]Departamento de Astrofísica, Universidad de La Laguna, La Laguna, Spain. [9]Lockheed Martin, Solar and Astrophysics Laboratory, Palo Alto, CA, USA. *e-mail: samuel.grant@qub.ac.uk

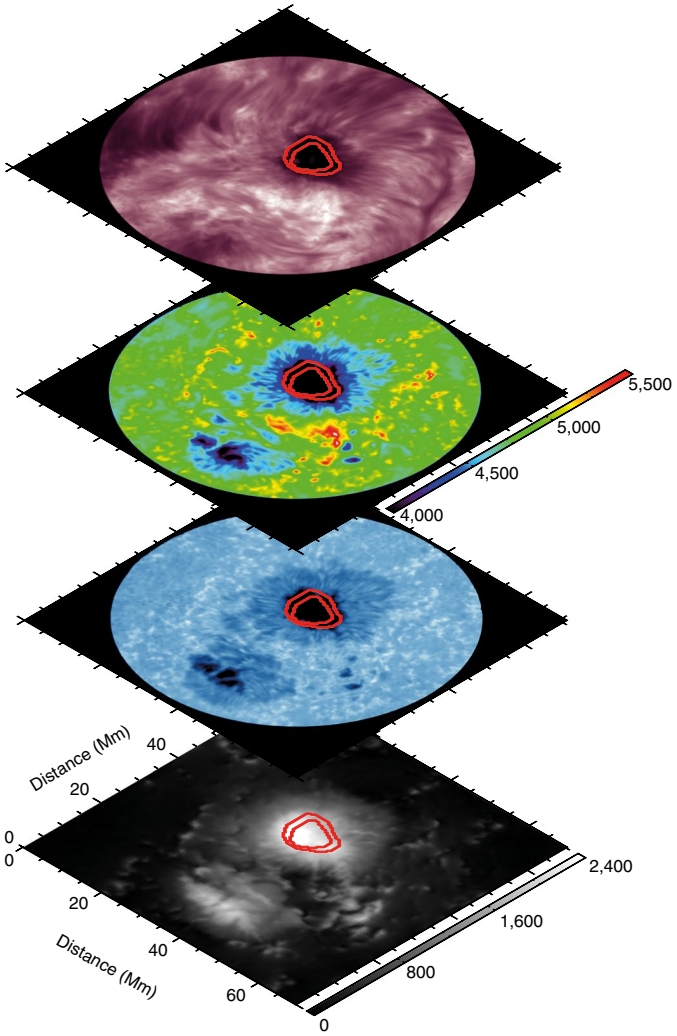

Fig. 1 | The building blocks of the magnetized solar atmosphere observed on 24 August 2014. Co-spatial images revealing the structure of the sunspot at 13:00 UT on 24 August 2014. The lower image shows the magnitude of the photospheric magnetic field from HMI, revealing high umbral field strengths (colour bar relates to the field strengths in gauss). The image above is taken from the blue wing of the Ca II 8,542 Å spectral line, displaying the photospheric representation of the sunspot. Above this is the photospheric plasma temperature of the region derived from CAISAR at $\log(\tau_{500nm}) \sim -2$ (or ~250 km above the photosphere), showing the clear temperature distinction between the umbra, penumbra and surrounding quiet Sun (colour bar in units of kelvin). The upper image shows the chromospheric core of the Ca II 8,542 Å spectral line, highlighting the strong intensity gradient between the umbra and penumbra at these heights. In each of these images, the red contours represent the inner and outer boundaries of the plasma-β=1 region at the height where shocks first begin to manifest (~250 km), where magneto-acoustic and Alfvén waves can readily convert.

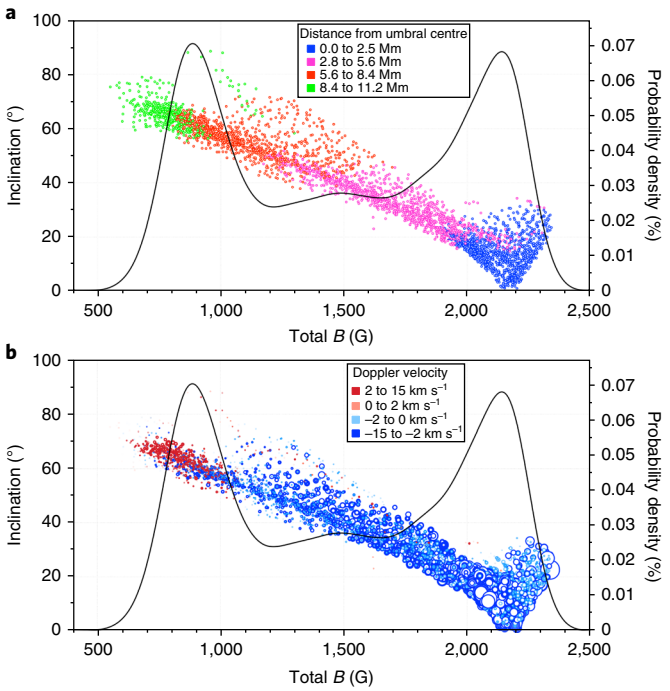

Fig. 2 | A statistical insight into the magnetic, velocity and occurrence relationships between shock phenomena in a sunspot umbra. a,**b**, The inclination of the magnetic field as a function of the total magnetic field strength for shock pixels at their point of formation, where an inclination of 0° represents an upwardly orientated vertical field. The colour scheme of the data points denotes their distance from the centre of the umbral core in Mm (**a**) and the LOS velocities of the resultant shock emission profiles, where positive values represent red-shifted plasma motion away from the observer, while negative values indicate blue-shifted plasma towards the observer (**b**). The diameters of the data points in **b** represent a visualization of the relative temperature increases of shocked plasma above their local quiescent background temperatures, where the largest circles represent significant temperature enhancements (up to a maximum of ~20%) that are synonymous with higher magnetic field strengths when compared to the smaller temperature enhancements associated with lower magnetic field strengths. The data points are over-plotted with the probability density function of shock occurrence as a function of the total magnetic field strength.

Alfvén wave shock formation. Alfvén shocks are predicted to form in regions with high negative Alfvén speed gradients[21], which is fulfilled by the volume expansion of the magnetic field lines and the highly inclined environment in which they exist, hence minimizing the effects of density stratification and promoting a negative gradient in the associated Alfvén speed.

The extrapolated vector magnetic fields are employed with the complementary CAlcium Inversion using a Spectral ARchive[22] (CAISAR) code, producing maps of magnetic and thermal pressure that are used to establish the physical locations where the ratio of these parameters, the plasma-β, equals unity (Fig. 1). Here, the plasma-β=1 region is analogous to the locations where the characteristic velocities of slow and fast waves are equal. Thus, ubiquitous magneto-acoustic waves throughout the umbra are capable of converting into Alfvén modes through the process of mode conversion[11,23]. This provides a bulk generation of Alfvén waves that can form both Alfvén and resonantly driven shocks under the correct atmospheric conditions. The magnetic topologies representative of the outermost boundary of the sunspot umbra provide such an environment where a steep negative Alfvén speed gradient is encountered by the propagating waves. UF shock formation in this regime is drastically suppressed due to the heavily inclined magnetic field lines providing substantially reduced density stratification along the paths of wave propagation.

Examination of the Doppler LOS velocities of the shocked plasma further distinguishes between UFs near the sunspot core and the Alfvén shocks at the periphery of the umbra. The LOS plasma velocities associated with the UF population are blue-shifted and display characteristic 'sawtooth' spectral profiles throughout their temporal evolution, consistent with the established morphology of UFs[24].

The second population, which dominates the outer umbral perimeter where the plasma-β equals unity, displays an intermingling of red- and blue-shifted plasma moving perpendicularly to the wave-vector (Fig. 2) during the onset of plasma shock events. This is in stark contrast to conventional UFs, and provides further direct evidence of Alfvén shocks, since large velocity excursions perpendicular to the vector magnetic field are representative of Alfvén waves undergoing nonlinear processes during the creation of shocks[21] (Fig. 3). Furthermore, the observed red-shifts indicate that approximately 70% of the observed shocks are due to the direct steepening of Alfvén waves, which is depicted in the right-hand side of Fig. 3.

Temporal analysis of the CAISAR inversions unveils how the strong dissipative thermal effects of the Alfvén shocks first appear just above the temperature minimum at $\log(\tau_{500\mathrm{nm}}) \sim -2$ (~ 250 km above the solar surface), where $\tau_{500\mathrm{nm}}$ represents the optical depth of the plasma at a wavelength of 500 nm. The greatest thermal perturbations occur between optical depths of $-5.3 < \log(\tau_{500\mathrm{nm}}) < -4.6$ ($\sim$750–1,100 km), corresponding to the low chromosphere[25]. Through comparison with the average background temperature, the Alfvén shocks are found to heat the localized plasma by $\sim 5\%$ (Fig. 4). By comparison, the ubiquitous slow magneto-acoustic shocks (UFs) identified at the cooler core of the sunspot umbra exhibit temperature increases on the order of 20% (lower panel of Fig. 2), consistent with previous estimations[13].

The wealth of high-resolution data allows for the calculation of the Alfvén wave energy flux that subsequently steepens into shocks. The energy flux, E_A, of an Alfvén wave can be expressed as

$$E_A = \rho v^2 c_A$$

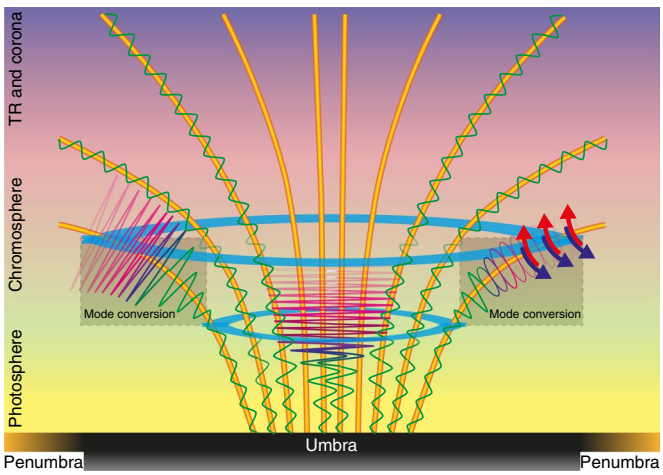

Fig. 3 | A cartoon representation of a sunspot umbral atmosphere demonstrating a variety of shock phenomena. A side-on perspective of a typical sunspot atmosphere, showing magnetic field lines (orange cylinders) anchored into the photospheric umbra (bottom of image) and expanding laterally as a function of atmospheric height, into the upper atmospheric regions of the transition region (TR) and corona. The light blue annuli highlight the lower and upper extents of the mode-conversion region for the atmospheric heights of interest. The mode-conversion region on the left-hand side shows a schematic of nonlinear Alfvén waves resonantly amplifying magneto-acoustic waves, increasing the shock formation efficiency in this location. The mode-conversion region on the right-hand side demonstrates the coupling of upwardly propagating magneto-acoustic oscillations (the sinusoidal motions) into Alfvén waves (the elliptical structures), which subsequently develop tangential blue- and red-shifted plasma during the creation of Alfvén shocks. The central portion represents the traditional creation of UFs that result from the steepening of magneto-acoustic waves as they traverse multiple density scale heights in the lower solar atmosphere. Image not to scale.

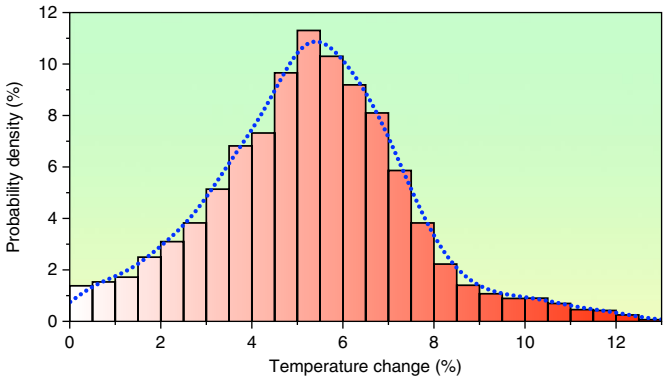

Fig. 4 | The distribution of temperature enhancements resulting from Alfvén shocks close to the umbral boundary. The probability density of percentage temperature perturbations derived from Alfvén shocks with respect to their average background temperature. The blue dotted line is a smoothed fit to the histogram, showing a clear peak at approximately 5%, which equates to the conversion of mechanical Alfvén wave flux into thermalized shock energy.

where $\rho = 3.57 \pm 1.30 \times 10^{-7}\,\mathrm{kg\,m^{-3}}$ is the density found from non-local thermodynamic equilibrium inversions[26], and $c_A = 6.2 \pm 0.5\,\mathrm{km\,s^{-1}}$ is the local Alfvén speed computed from the vector magnetic field extrapolations, with both values computed at the atmospheric height and outer umbral location synonymous with the Alfvén shock detections ($\log(\tau_{500\mathrm{nm}}) \sim -5$ within the plasma-$\beta = 1$ isocontours in Fig. 1). The calculated Alfvén speed is also consistent with modern statistical seismological findings[27]. A velocity amplitude, $v = 2.2 \pm 0.6\,\mathrm{km\,s^{-1}}$, is computed from the average absolute velocity values related to the Alfvén wave population displayed in Fig. 2. These measurements, derived directly from the observations, output an Alfvén energy flux of $E_A = 10.7 \pm 5.7\,\mathrm{kW\,m^{-2}}$. This energy is substantially less than the $20\,\mathrm{kW\,m^{-2}}$ observed for upwardly propagating magneto-acoustic waves generated in photospheric sunspot umbrae[28]. Such a differential is not unexpected, as only a portion of the photospheric flux will mode-convert into Alfvén waves within the $\beta = 1$ layer[29]. Furthermore, partially ionized atoms that make up the cool umbral chromosphere will naturally absorb a significant portion of the available energy through ionization and ion-neutral processes above the temperature minimum[30]. Hence, only a fraction of the initial energy will directly contribute to the observed temperature increase of $\sim 5\%$, thus remaining consistent with the scenario of magneto-acoustic mode conversion leading to the steepening of Alfvén waves into shock fronts.

Here, we show the dissipation of chromospheric Alfvén waves into thermal energy for the first time. We reveal how high-resolution observations provide the direct detection of these signatures, in the form of identifying the necessary plasma-$\beta = 1$ equipartition region and revealing the co-spatial negative Alfvén speed gradients and associated tangential Doppler velocities synonymous with Alfvén shock dissipation, to provide first light on an enigmatic problem within astrophysics that has remained elusive for over half a century. With the viability of Alfvén waves to heat localized plasma confirmed, future studies can build upon our novel findings and examine the consequences of Alfvén shocks in greater detail using spectro-polarimetric data and advanced inversion techniques. Looking further ahead, the capabilities of the upcoming 4 m Daniel K. Inouye Solar Telescope, set for first light in 2019, will unveil the fine structure of these shocks on an unprecedented scale, allowing the role Alfvén shocks play in global solar atmospheric heating to be fully assessed.

Methods

Methods, including statements of data availability and any associated accession codes and references, are available at https://doi.org/10.1038/s41567-018-0058-3.

Received: 3 April 2017; Accepted: 24 January 2018;
Published online: 05 March 2018

References

1. Alfvén, H. Magneto hydrodynamic waves, and the heating of the solar corona. *Mon. Not. R. Astron. Soc.* **107**, 211–219 (1947).
2. Gekelman, W., Vincena, S., Leneman, D. & Maggs, J. Laboratory experiments on shear Alfvén waves and their relationship to space plasmas. *J. Geophys. Res.* **102**, 7225–7236 (1997).
3. Mathioudakis, M., Jess, D. B. & Erdélyi, R. Alfvén waves in the solar atmosphere. From theory to observations. *Space Sci. Rev.* **175**, 1–27 (2013).
4. Morton, R. J., Verth, G., Fedun, V., Shelyag, S. & Erdélyi, R. Evidence for the photospheric excitation of incompressible chromospheric waves. *Astrophys. J.* **768**, 17 (2013).
5. Beckers, J. M. & Tallant, P. E. Chromospheric inhomogeneities in sunspot umbrae. *Sol. Phys.* **7**, 351–365 (1969).
6. Jess, D. B. et al. Multiwavelength studies of MHD waves in the solar chromosphere. An overview of recent results. *Space Sci. Rev.* **190**, 103–161 (2015).
7. Tomczyk, S. et al. Alfvén waves in the solar corona. *Science* **317**, 1192–1196 (2007).
8. De Pontieu, B. et al. Chromospheric Alfvén waves strong enough to power the solar wind. *Science* **318**, 1574–1577 (2007).
9. Jess, D. B. et al. Alfvén waves in the lower solar atmosphere. *Science* **323**, 1582–1585 (2009).
10. Heyvaerts, J. & Priest, E. R. Coronal heating by phase-mixed shear Alfvén waves. *Astron. Astrophys.* **117**, 220–234 (1983).
11. Bogdan, T. J. et al. Waves in the magnetized solar atmosphere. II. Waves from localized sources in magnetic flux concentrations. *Astrophys. J.* **599**, 626–660 (2003).
12. Schwarzschild, M. On noise arising from the solar granulation. *Astrophys. J.* **107**, 1–5 (1948).
13. de la Cruz Rodrguez, J., Rouppe van der Voort, L., Socas-Navarro, H. & van Noort, M. Physical properties of a sunspot chromosphere with umbral flashes. *Astron. Astrophys.* **556**, A115 (2013).
14. Arber, T. D., Brady, C. S. & Shelyag, S. Alfvén wave heating of the solar chromosphere: 1.5D models. *Astrophys. J.* **817**, 94 (2016).
15. Montgomery, D. Development of hydromagnetic shocks from large-amplitude Alfvén waves. *Phys. Rev. Lett.* **2**, 36–37 (1959).
16. Hada, T. Evolution of large amplitude Alfvén waves in the solar wing with beta approximately 1. *Geophys. Res. Lett.* **20**, 2415–2418 (1993).
17. Cavallini, F. IBIS: A new post-focus instrument for solar imaging spectroscopy. *Sol. Phys.* **236**, 415–439 (2006).
18. Wiegelmann, T. Nonlinear force-free modelling of the solar coronal magnetic field. *J. Geophys. Res.* **113**, A03S02 (2008).
19. Schou, J. et al. Design and ground calibration of the Helioseismic and Magnetic Imager (HMI) instrument on the Solar Dynamics Observatory (SDO). *Sol. Phys.* **275**, 229–259 (2012).
20. Bard, S. & Carlsson, M. Radiative hydrodynamic simulations of acoustic waves in sunspots. *Astrophys. J.* **722**, 888 (2010).
21. Hollweg, J. V., Jackson, S. & Galloway, D. Alfvén waves in the solar atmosphere. III – Nonlinear waves on open flux tubes. *Sol. Phys.* **75**, 35–61 (1982).
22. Beck, C., Choudhary, D. P., Rezaei, R. & Louis, R. E. Fast inversion of solar Ca ii spectra. *Astrophys. J.* **798**, 100 (2015).
23. Khomenko, E. & Cally, P. S. Numerical simulations of conversion to Alfvén waves in sunspots. *Astrophys. J.* **746**, 68 (2012).
24. Rouppe van der Voort, L. H. M., Rutten, R. J., Sütterlin, P., Sloover, P. J. & Krijger, J. M. La Palma observations of umbral flashes. *Astron. Astrophys.* **403**, 277–285 (2003).
25. Maltby, P. et al. A new sunspot umbral model and its variation with the solar cycle. *Astrophys. J.* **306**, 284–303 (1986).
26. Socas-Navarro, H., de la Cruz Rodrguez, J., Asensio Ramos, A., Trujillo Bueno, J. & Ruiz Cobo, B. An open-source, massively parallel code for non-LTE synthesis and inversion of spectral lines and Zeeman-induced Stokes profiles. *Astron. Astrophys.* **577**, A7 (2015).
27. Cho, I.-H. et al. Determination of the Alfvén speed and plasma-beta using the seismology of sunspot umbra. *Astrophys. J. Lett.* **837**, L11 (2017).
28. Kanoh, R., Shimizu, T. & Imada, S. Hinode and IRIS observations of the magnetohydrodynamic waves propagating from the photosphere to the chromosphere in a sunspot. *Astrophys. J.* **831**, 24 (2016).
29. Cally, P. S. & Moradi, H. Seismology of the wounded Sun. *Mon. Not. R. Astron. Soc.* **435**, 2589–2597 (2013).
30. Fontenla, J. M., Curdt, W., Haberreiter, M., Harder, J. & Tian, H. Semiempirical models of the solar atmosphere. III. Set of non-LTE models for the far-ultraviolet/extreme-ultraviolet irradiance computation. *Astrophys. J.* **707**, 482–502 (2009).

Acknowledgements

S.D.T.G. and S.J.H. thank the Northern Ireland Department for Employment and Learning (now the Northern Ireland Department for the Economy) for the awards of PhD studentships. D.B.J. wishes to thank the UK Science and Technology Facilities Council for the award of an Ernest Rutherford Fellowship alongside a dedicated Research Grant. S.D.T.G. and D.B.J. also wish to thank Invest NI and Randox Laboratories Ltd for the award of a Research & Development Grant (059RDEN-1) that allowed this work to be undertaken. T.Z. was supported by the Austrian Science Fund (FWF) project P30695-N27 and by the Georgian Shota Rustaveli National Science Foundation project DI-2016-17. H.S.-N. acknowledges support from the Spanish Ministry of Economy and Competitivity through project AYA2014-60476-P (Solar Magnetometry in the Era of Large Solar Telescopes). P.H.K. is grateful to the Leverhulme Trust for the award of an Early Career Fellowship. The NSO is operated by the Association of Universities for Research in Astronomy under cooperative agreement with the National Science Foundation. The magnetic field measurements employed in this work are courtesy of NASA/SDO and the AIA, EVE and HMI science teams.

Author contributions

S.D.T.G., D.B.J. and P.H.K. performed analysis of the observations. S.D.T.G., D.B.J., T.V.Z., M.J.A., D.J.C., S.J.H. and R.L.H. interpreted the observations. S.D.T.G, D.B.J., C.B., H.S.-N. and M.J.A. prepared and processed all data products. All authors discussed the results and commented on the manuscript.

Competing interests

The authors declare no competing interests.

Additional information

Supplementary information is available for this paper at https://doi.org/10.1038/s41567-018-0058-3.

Reprints and permissions information is available at www.nature.com/reprints.

Correspondence and requests for materials should be addressed to S.D.T.G.

Publisher's note: Springer Nature remains neutral with regard to jurisdictional claims in published maps and institutional affiliations.

Methods

Sunspot observations. The focus of the study was the sunspot at the centre of the active region NOAA 12146 on 24 August 2014. The spectral data was acquired with the Interferometric BIdimensional Spectrometer[17] (IBIS), at the Dunn Solar Telescope, New Mexico, USA. IBIS sampled the Ca II absorption profile at 8,542.12 Å at 27 non-equidistant wavelength steps. After processing, the data had an effective spatial sampling of 0.098″ (71 km) per pixel and a temporal cadence of 5.8 s per full scan, for a total of 1,336 spectral imaging cubes.

Complementary vector magnetograms of the same active region were collected from the Helioseismic and Magnetic Imager[19] (HMI), aboard the Solar Dynamics Observatory[31] (SDO) spacecraft, with a time cadence of 720 s and a two-pixel spatial resolution of 1.0″ (725 km). Further information on these data products can be found in Section 1 of the Supplementary Material.

Magnetic field extrapolations. Magnetic field extrapolations were conducted on the outputs of the Very Fast Inversion of the Stokes Vector[32] (VFISV) algorithm applied to the HMI observations. A nonlinear force-free field extrapolation code[18] was applied to the derived heliographic components[33,34], providing information related to the vector magnetic field as a function of atmospheric height. The final outputs of the extrapolations were converted into key parameters for the present study, namely the transverse (B_{trans}) and total (B_{tot}) magnetic field strengths, in addition to the inclination and azimuth angles, all as a function of atmospheric height.

The chromospheric outputs of the extrapolations were validated and verified through their comparison to a vertical current approximation magnetic field extrapolation code[35], which employed tracked and isolated features captured by complementary Hα observations of the region of interest obtained with the Hydrogen-Alpha Rapid Dynamics camera[36] (HARDcam). Further discussion of the techniques and considerations necessary for the application of the extrapolations can be found in Section 2 of the Supplementary Material.

Detecting umbral shocks. Shocks were isolated within the IBIS observations by creating running-mean-subtracted images of the chromospheric line core data, allowing the intensity contrasts of the shock events to be improved[24,37]. The sunspot umbra was also isolated from the penumbra by means of intensity thresholding. The resultant umbral time series, taken at the rest wavelength of 8,542.12 Å, had the calculated mean for each time step over ±25 images subtracted, corresponding to an approximate 5 minute window. The only exceptions were the first and last 25 images, where this was impossible. For these images, the mean of the first and last 50 images, respectively, were subtracted[37].

Shock pixels were visually assessed to be any umbral pixel in the mean subtracted maps exhibiting an intensity excursion exceeding 2.7σ above zero, where σ is the standard deviation of the mean subtracted map. Using this threshold, 554,792 UF pixels were detected within the 135 minute image sequence. This methodology is considered further in Section 3 of the Supplementary Material.

Doppler velocity of shocks. The chromospheric emission, resulting from the presence of shocked plasma, perturbs the shapes of the quiescent Ca II 8,542 Å spectral profiles, making the calculations of the line-of-sight (LOS) Doppler velocities more complex. In this study, the LOS velocities are derived from resultant emission profiles, created by subtracting the time-averaged spectral profile at each location from the spectra evident during the detected shock. The resultant spectra take the form of emission profiles representing the spectral characteristics of the shocked plasma at that particular instant. Subsequently, the LOS velocities are calculated using cumulative distribution functions of intensity against wavelength[38], where the line core is defined as the wavelength where 50% of the emission has occurred. The implications of this method are considered in Section 5 of the Supplementary Material.

Deriving the shocked plasma temperature. The thermal structuring of the entire active region is derived using the CAlcium Inversion using a Spectral ARchive[39] (CAISAR) code developed specifically for the Ca II intensity profiles obtained from IBIS observations. This method employs a local thermodynamic equilibrium (LTE) atmosphere and derives the thermal properties through the comparison of the observed profiles to a synthesized archive encompassing a large variety of temperature perturbations[40–42]. A first-order correction to a non-LTE environment has been established and verified[22], allowing for accurate chromospheric temperature differentials to be derived from a corrected LTE framework in a timely manner. The accuracy of these inversions is discussed in Section 6 of the Supplementary Material.

Ascertaining the plasma density. In order to establish the plasma-$\beta = 1$ regions within the atmospheric column of the sunspot, and also to deduce the properties of the identified Alfvén waves subsequently forming shock fronts, it is necessary to infer the plasma densities of the umbra at various atmospheric heights. For the plasma-β calculations, a semi-empirical model is used[25] that allows the intrinsic stratification of the densities to be accounted for, providing robust approximations for the plasma densities throughout the lower atmosphere of the sunspot. The implications of applying a semi-empirical model are discussed in Section 9 of the Supplementary Material.

In order to infer the densities at the specific spatial locations of the Alfvén shocks, it was prudent to employ the most accurate method currently available, which ensures the resulting energy calculations are accurate. To that end, the Non-LTE Inversion Code using the Lorien Engine[26] (NICOLE) was applied to a selection of 200 profiles associated with Alfvén shocks. The non-LTE inversions with NICOLE require several seconds per profile, and thus could not be run over all 10^9 sampled Ca II 8,542 Å spectra in a reasonable time. The reduced sample size allowed for NICOLE to be run with a large number of nodes in order to best reproduce the rich structuring of the chromospheric Ca II 8,542 Å line profiles observed in the data.

Data availability. The data used in this paper are from the observing campaign entitled 'Nanoflare Activity in the Lower Solar Atmosphere' (NSO-SP proposal T1020; Principal Investigator: D. B. Jess), which employed the ground-based Dunn Solar Telescope, USA, during August 2014. Additional supporting observations were obtained from the publicly available NASA Solar Dynamics Observatory (https://sdo.gsfc.nasa.gov) data archive, which can be accessed via http://jsoc.stanford.edu/ajax/lookdata.html. The ground-based data obtained during 24 August 2014 is several TB in size, and cannot be hosted on a public server. However, all data supporting the findings of this study are available directly from the authors on request.

References

31. Pesnell, W. D., Thompson, B. J. & Chamberlin, P. C. The Solar Dynamics Observatory (SDO). *Sol. Phys.* **275**, 3–15 (2012).
32. Borrero, J. M. et al. VFISV: Very Fast Inversion of the Stokes Vector for the Helioseismic and Magnetic imager. *Sol. Phys.* **273**, 267–293 (2011).
33. Metcalf, T. R. et al. An overview of existing algorithms for resolving the 180° ambiguity in vector magnetic fields: Quantitative tests with synthetic data. *Sol. Phys.* **237**, 267–296 (2006).
34. Leka, K. D. et al. Resolving the 180° ambiguity in solar vector magnetic field data: Evaluating the effects of noise, spatial resolution, and method assumptions. *Sol. Phys.* **260**, 83–108 (2009).
35. Aschwanden, M. J. The vertical-current approximation nonlinear force-free field code - Description, performance tests, and measurements of magnetic energies dissipated in solar flares. *Astrophys. J. Supp.* **224**, 25 (2016).
36. Jess, D. B. et al. The source of 3 minute magnetoacoustic oscillations in coronal fans. *Astrophys. J.* **757**, 160 (2012).
37. Madsen, C. A., Tian, H. & DeLuca, E. E. Observations of umbral flashes and running sunspot waves with the Interface Region Imaging Spectrograph. *Astrophys. J.* **800**, 129 (2015).
38. Kerr, G. S., Simões, P. J. A., Qiu, J. & Fletcher, L. IRIS observations of the Mg II H and K lines during a solar flare. *Astron. Astrophys.* **582**, A50 (2015).
39. Rezaei, R. & Beck, C. Multiwavelength spectropolarimetric observations of an Ellerman bomb. *Astron. Astrophys.* **582**, A104 (2015).
40. Beck, C., Rezaei, R. & Puschmann, K. G. The energy of waves in the photosphere and lower chromosphere. III. Inversion setup for Ca ii H spectra in local thermal equilibrium. *Astron. Astrophys.* **549**, A24 (2013).
41. Beck, C., Rezaei, R. & Puschmann, K. G. The energy of waves in the photosphere and lower chromosphere. IV. Inversion results of Ca ii H spectra. *Astron. Astrophys.* **553**, A73 (2013).
42. Beck, C., Choudhary, D. P. & Rezaei, R. A three-dimensional view of the thermal structure in a super-penumbral canopy. *Astrophys. J.* **788**, 183 (2014).